

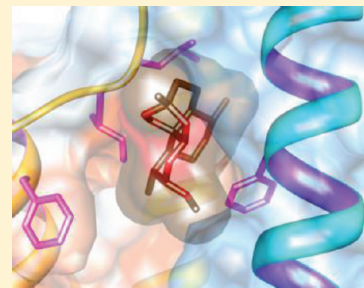
Identification of the *Schistosoma mansoni* Molecular Target for the Antimalarial Drug Artemether

Rosalba Lepore,[†] Silvia Simeoni,[†] Domenico Raimondo,[†] Antonia Caroli,[†] Anna Tramontano,^{*,†,‡} and Allegra Via^{*,†}

[†]Department of Physics and [‡]Istituto Pasteur Fondazione Cenci Bolognetti, Sapienza University of Rome, Rome, Italy

S Supporting Information

ABSTRACT: *Plasmodium falciparum* and *Schistosoma mansoni* are the parasites responsible for most of the malaria and schistosomiasis cases in the world. Notwithstanding their many differences, the two agents have striking similarities in that they both are blood feeders and are targets of an overlapping set of drugs, including the well-known artemether molecule. Here we explore the possibility of using the known information about the mode of action of artemether in *Plasmodium* to identify the molecular target of the drug in *Schistosoma* and provide evidence that artemether binds to SmSERCA, a putative Ca^{2+} -ATPase of *Schistosoma*. We also predict the putative binding mode of the molecule for both its *Plasmodium* and *Schistosoma* targets. Our analysis of the mode of binding of artemether to Ca^{2+} -ATPases also provides an explanation for the apparent paradox that, although the molecule has no side effect in humans, it has been shown to possess antitumoral activity.



INTRODUCTION

Malaria and schistosomiasis are two of the most important parasitic diseases in humans, resulting in significant mortality and devastating social and economic consequences.

Malaria affects ~300 million people each year, and about 200 million people are chronically infected with schistosomiasis. In many areas of the world, the two diseases are co-endemic and therefore coinfections are common. Malaria is caused by a unicellular parasite of the genus *Plasmodium* that is spread from person to person through the bites of infected mosquitoes, usually belonging to the *Anopheles* genus. If not promptly treated with effective drugs, malaria can cause severe illness and is often fatal. Five species cause malaria in humans: *Plasmodium falciparum*, *P. vivax*, *P. ovale*, *P. malariae*, and *P. knowlesi*. Among them *P. falciparum* is the most virulent, spread and deadly. The life cycle of the *Plasmodium* is extraordinarily complex requiring specialized protein expression, therefore drugs will be most effective if targeted at specific parasite life stages and/or specific protein expressed at these stages.

Schistosomiasis is caused by a platyhelminth of the genus *Schistosoma*, which has a complex parasitic lifecycle, involving two obligatory hosts, a freshwater mollusc and a mammal. There are four species infecting humans: *Schistosoma mansoni*, *S. hematobium*, *S. japonicum*, and *S. intercalatum*; among them, *S. mansoni* is the widest spread, and *S. japonicum* is the most virulent. Both malaria and schistosomiasis parasites are blood feeders.

Current therapies against malaria are mainly based on quinine, chloroquine, and artemisinins, while praziquantel is the current mainstay for morbidity control of schistosomiasis. Interestingly praziquantel has been suggested as a new line for

treatment of malaria,¹ whereas artemisinins are known to have antischistosomal properties.²

In summary, both parasites are blood feeders and are targets of an overlapping set of therapeutic molecules. The latter observation creates both a problem and an opportunity. On one side, their co-presence in the same geographical areas and the overlap between their therapies poses serious problems in fighting the onset of drug resistance in both cases, and on the other, the knowledge gained on one parasite can be exploited for improving our chances to fight the other and vice versa. In particular, the knowledge of an effective drug against one parasite can be used as starting point for developing a molecule inhibiting the analogous target in the other, and at the same time, the knowledge of the target (or receptor) of a drug in one parasite can lead to the identification of the unknown target for the same or a similar molecule in the other.

This is the strategy we are following, and in this paper we describe our results on artemether, an active methyl ether derivative of artemisinin (Figure 1), which is a sesquiterpene endoperoxide isolated from *Artemisia annua*. Artemisinin and its derivatives are structurally distinct from other antimalarial drugs. The inhibition mechanism of these compounds is based on the breaking of the trioxane pharmacophore peroxide bridge, which is essential for their antimalarial activity.³ All members of this class of compounds, including artemisinin and artemether, produce dihydroartemisinin as a reaction intermediate. Artemether is more stable and soluble than artemisinin,⁴ it is known to kill *P. falciparum* by specifically inhibiting *PfATP6*⁵ ($K_i \sim 0.5\text{--}2 \mu\text{M}$), the parasite homologue of

Received: April 19, 2011

Published: October 13, 2011

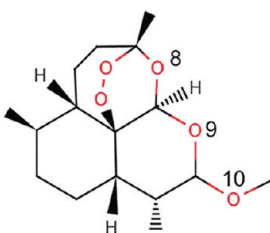


Figure 1. Artemether atomic structure. The molecule was drawn using Marvin 5.3.3, 2010, ChemAxon (<http://www.chemaxon.com>, accessed March 2, 2011).

the sarco/endoplasmic reticulum Ca^{2+} -ATPases (SERCAs) (twice more effectively than artemisinin)⁶ and is also one of the first drugs observed to inhibit *S. mansoni*.²

In line with our reasoning, we used state of the art computational and docking techniques to try and identify the molecular target of artemether in *Schistosoma*. We provide strong support to the hypothesis that the homologue of *PfATP6* in *Schistosoma*, *SmSERCA*, is the molecular target of artemether in this parasite.

Furthermore, by computationally analyzing the putative mode of binding of artemether to the human SERCA homologue, we also propose a mechanism able to rationalize the different pharmacological activity of artemether in the parasites and in humans and to explain an apparent paradox. In fact, in humans the intake of the molecule has no noticeable side effects⁷ and Eckstein-Ludwig et al⁵ observed that mammalian SERCAs are not inhibited by artemisinins. However, some authors reported selective toxicity of artemisinins, including artemether,⁸ toward human cancer cells.^{9–11}

MATERIALS AND METHODS

Homology Modeling. The sequences of *SmSERCA* (UniProt accession number: C4Q4H9) and *PfATP6* (UniProt accession number: Q5R2K6) were obtained from the UniProt database (<http://www.uniprot.org>, accessed March 2, 2011) and comprise 1148 and 1228 amino acids, respectively, whereas the sequence of human SERCA is 994 amino acids long. To detect suitable structural templates for the target proteins, we used the HHpred software (<http://toolkit.tuebingen.mpg.de/hhpred>),¹² which is a sensitive homology detection tool.¹³ The search for templates was performed against the PDB database.¹⁴ The best template found for all three proteins is the sarcoplasmic/endoplasmic reticulum calcium ATPase of *Oryctolagus cuniculus*, *OcSERCA* (73% sequence identity, *E*-value $<1.3 \times 10^{-40}$, 48% sequence identity, *E*-value $<1.4 \times 10^{-45}$ and 97% sequence identity, *E*-value $<4.2 \times 10^{-45}$ for *SmSERCA*, *PfATP6*, and *HsSERCA*, respectively). Target-template sequence alignments are reported in Figure S2, Supporting Information. The *OcSERCA* crystal structure is available in a calcium-bound form (E1- Ca^{2+} state, PDB: 1SU4) and in a calcium-free form in the presence of thapsigargin (TG), a potent inhibitor of the enzyme (E2-TG state, PDB: 2AGV). This made it possible to build two different models for our target proteins corresponding to the E1 and E2 conformational states.

The target-template sequence identity between *OcSERCA* and *SmSERCA* is 73%. The C-term tail of 88 residues has not been modeled because no template is available for this region. Two models, one for state E1 and one for state E2, were obtained using the spatial restraint-based method implemented in the

MODELLER software.¹⁵ We generated 50 models for each conformational state. The best model for each conformational state was selected on the basis of the MODELLER objective function.

In order to model the insertion that occurs in the cytoplasmic domain of the protein (Val508 to Glu516), 20 loop conformations were generated by the loopmodel tool of MODELLER. The best loop model was chosen based on the DOPE statistical potential score.¹⁶ The final models were evaluated using the ProQM model quality assessment program.¹⁷

The sequence identity between *PfATP6* and *OcSERCA* is 48%. The *PfATP6* sequence contains two long low-complexity insertions (from Leu382 to Arg473 and from Asn569 to Cys677) that are expected to be intrinsically disordered and were not modeled. The target-template sequence alignment was manually modified by removing the insertion regions, and the final alignment was used as input for MODELLER. Also in this case, the protein was modeled in two different conformational states using as templates the crystal structures from rabbit in state E1 (PDB: 1SU4) and E2 (PDB: 2AGV), respectively. Also in this case, 50 models were built for each conformational state, and the final models, selected on the basis of the MODELLER objective function, were evaluated using the ProQM model quality assessment program.¹⁷

Human SERCA shares 97% sequence identity with *OcSERCA*. Also in this case the model was built using MODELLER.

All the models built in this work have been deposited in the Protein Model Data Base PMDB¹⁸ and can be retrieved using the following IDs: PM0077298 (*PfATP6* in state E1), PM0077299 (*PfATP6* in state E2), PM0077300 (*SmSERCA* in state E1), PM0077301 (*SmSERCA* in state E2), PM0077302 (*HsSERCA* in state E1), and PM0077303 (*HsSERCA* in state E2).

The root-mean-square deviation (rmsd) of the superimposed three-dimensional models in E1 and E2 conformations is very similar to the rmsd of the superimposed *OcSERCA* crystal structures in E1 and E2 conformations (14.015 Å), namely 14.047 Å (*S. mansoni*), 14.256 Å (*P. falciparum*), and 14.262 Å (*H. sapiens*). This large conformational change between the Ca^{2+} -bound and -unbound states of the protein has been extensively described by Toyoshima and Nomura who solved the crystal structure of SERCA in both states.^{19,20} Upon calcium binding, 6 of the 10 transmembrane helices undergo large-scale rearrangements, while the cytoplasmic domains gather to form a compact cluster, thus ensuring both that calcium can be released into the lumen of sarcoplasmic reticulum and that, on the cytoplasmic side, a pathway for entry of new calcium ions is created.

Artemether Coordinates. The molecular structure of artemether was retrieved from the Cambridge Structural Database (CSD), the world repository of small molecule crystal structures.²¹

Molecular Docking. The procedure that we used to identify ligand preferential binding sites in the protein structures consisted of two steps: (i) “blind” docking, i.e., coarse grained unbiased search for putative binding site on the whole protein surface; and (ii) “site-specific” docking, where the sites selected in the first step are searched more finely to find the best orientation of the docked molecule in the binding site.

Docking experiments were performed using AutoDock4.2.²²

Nonprotein components, such as water molecules, inhibitors, and metal ions, were manually deleted from the X-ray crystal structures, whereas hydrogen atoms were added to the protein using the Chimera software.²³ AutoDock runs were performed using a compilation of Python scripts released by The Scripps

Table 1. Parameters Used in the Blind Docking Experiments

protein	n pts (<i>x, y, z</i>)	grid spacing (Å)	grid center coords	genetic algorithm runs	genetic algorithm evaluations
PfATP6	160, 250, 160	0.375	1.09, 0.45, 31.31	200	25 000 000
SmSERCA	160, 250, 160	0.375	1.93, 1.49, 31.51	200	25 000 000
HsSERCA	160, 250, 160	0.375	1.81, 1.20, 31.42	200	25 000 000

Research Institute (<http://autodock.scripps.edu/>). The AutoDock-Tools package, i.e., the free graphical user interface (GUI) of AutoDock, was used to create the simulation grid box. Blind docking experiments were carried out by placing the whole protein into the simulation box, the dimensions of which were set to $160 \times 250 \times 160$ grid points. In order to expand the simulation box dimensions, some AutoDock scripts (*autogpfCommands.py*; *GridParameters.py*) were manually modified, and the program was recompiled. Other parameter settings were: grid spacing: 0.375 Å; genetic algorithm runs: 200; and genetic algorithm number of evaluations: 25 000 000. All other parameters were set at their default values.

A cluster analysis was performed on all docking results: All docked conformations were compared with one another based on the positional rmsd of corresponding atoms. The resulting families of conformations were ranked according to increasing energy values. The Autodock default value of 2.0 Å was used as rmsd threshold for the structural comparison of conformations. Finally, the conformation with the lowest free energy of binding from the most populated cluster was used for the subsequent site-specific docking step. In the latter procedure, performed to obtain a finer sampling of the ligand orientations, the grid box was centered on the center of mass of the ligand in the pose obtained in the blind docking step. The number of points in each direction was set to 75 and the point spacing to 0.375 Å. Other parameters, such genetic algorithm runs and genetic algorithm number of evaluations, were the same as in the blind docking experiments.

Table 1 shows the parameters used for the docking simulations. The “best scoring ligand” is the one corresponding to the conformation with the lowest free energy of binding from the most populated cluster.

■ RESULTS AND DISCUSSION

Target Proteins. Mammalian SERCAs are Ca^{2+} pumps residing in the sarco/endoplasmic reticulum and involved in intracellular Ca^{2+} signaling. PfATP6 resides in the parasite endoplasmic reticulum and has a similar functional role. Eckstein-Ludwig and collaborators experimentally observed that the inhibition of PfATP6 by artemisinins is Fe^{2+} -dependent⁵ and suggested that the mechanism for the antimalarial action of artemisinins is explained by the production of carbon-centered free radicals following the interaction between Fe^{2+} and the artemisinin endoperoxide bridge, a key structural feature of the molecule.

It has been reported²⁴ that a single amino acid mutation is likely to be responsible for the difference in sensitivity to artemisinins of PfATP6 and of its mammalian homologue SERCAs: The mammalian SERCAs contain a glutamic acid at position 255, a position occupied by Leu in the *plasmodium* PfATP6. The single Leu to Glu mutation at this position in PfATP6 (Leu263Glu), abolishes sensitivity to artemisinins. Interestingly, nevertheless, parasite clones expressing wild-type or Leu263Glu variant PfATP6 show no significant difference in the IC_{50} inhibition concentrations of artemisinin and its derivatives

dihydroartemisinin and artesunate, although a trend toward reduced susceptibility was observed with low statistical significance ($p \approx 0.1$).²⁵

The crystal structure of PfATP6 and SmSERCA has not been experimentally determined, however, the X-ray crystal structure of a mammalian SERCA protein (from rabbit) is known in two conformations (PDB code: 1SU4 and 2AGV) (Figure 2a and b). The two forms represent the calcium-bound and -free conformations, respectively, and, from a structural point of view, differ by the relative orientation of the three cytoplasmic domains and by the spatial arrangement of their transmembrane helices. The rmsd of the structural superimposition of the two conformers is 14.015 Å.

Both mammalian and parasite SERCAs are known to be potently inhibited by TG (OcSERCA: $K_i \sim 64 \text{ nM}$,⁵ PfATP6: $K_i \sim 146 \pm 66 \text{ nM}$,⁵ and SmSERCA: $\text{IC}_{50} = 250 \pm 50 \text{ nM}$)²⁶ (Figure 3), which, similarly to artemether, is a sesquiterpene compound. Both mutational studies²⁴ and fluorescence assays⁵ suggest that artemisinins bind PfATP6 in the same region where TG binds mammalian SERCAs, namely a cavity surrounded by the M3, M5, and M7 transmembrane helices (Figure 2b), hereafter referred to as the TG-binding cavity. TG binds to SERCAs in the calcium free form and inhibits the enzymes by preventing them from changing conformation. The calcium free form has been solved in complex with the TG inhibitor (Figure 3).

Competition in the binding of PfATP6 was experimentally observed between artemisinin and TG.⁵ This experiment showed that both artemisinin and TG bind to a similar site of the two parasite proteins.

Whether this holds for artemether and whether the artemether-bound enzyme is in the calcium free form is less clear. For this reason, we modeled SERCAs in both calcium-bound and -free conformations and carried out docking studies on both forms.

PfATP6 and SmSERCA Template Selection and Modeling. The mammalian protein can be effectively used as a template to build a homology model of the two parasite proteins since the PfATP6 and SmSERCA sequences share 48% and 73% sequence identity with the mammalian one, respectively (Figure 4).

It should be mentioned that a three-dimensional model of PfATP6 in the calcium-bound E1 conformation has been previously described.²⁴ The model, stored in the PDB with the code 1U5N, was based on an old, deprecated, rabbit template (PDB: 1EUL; resolution, 2.6 Å), and therefore, we selected to build a new one taking advantage of more recently determined and more accurate template structures now available for both the E1 and E2 states.

As it can be appreciated from Figure 4, the PfATP6 sequence contains two long insertions with respect to the mammalian proteins. The low complexity composition of their sequences indicates that they are very likely to be intrinsically disordered, and accordingly, they are predicted to be so by the DISOPRED2 and IUPRED servers.^{27,28} It follows that they are not expected to be part of the core of the structure, hence our models do not

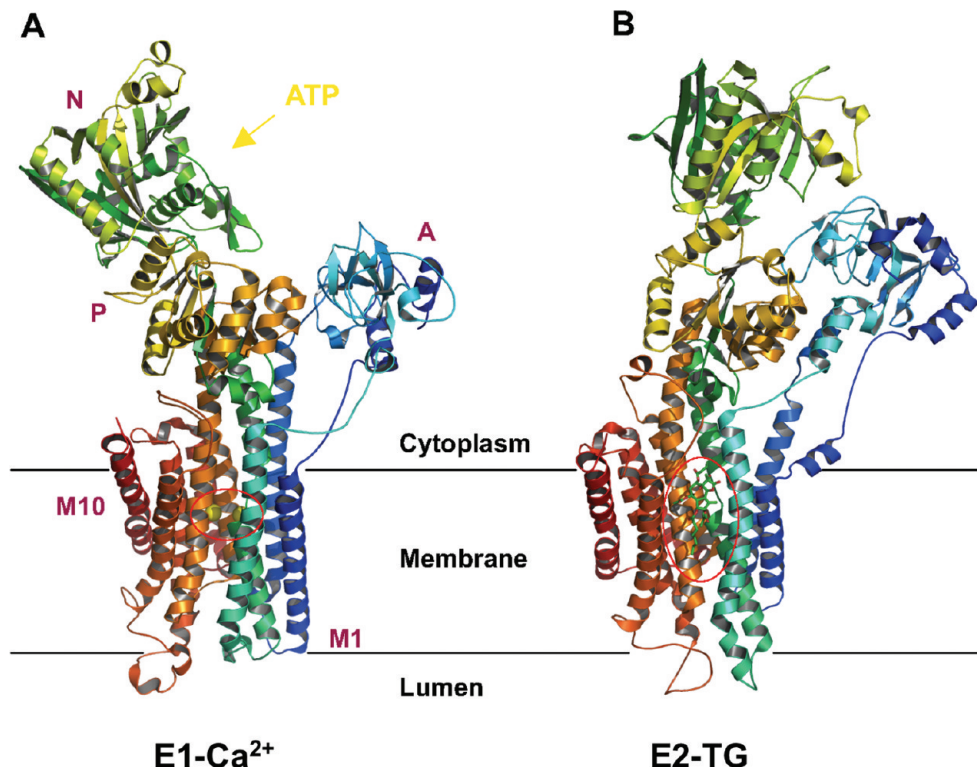


Figure 2. Three-dimensional structures of OcSERCA in the E1 and E2 conformations. (A) The OcSERCA structure in the calcium-bound state E1 (PDB: 1SU4). The red circle indicates the calcium binding site. Calcium is represented by green spheres. (B) The OcSERCA structure in the calcium-free state E2 (PDB: 2AGV). The red circle indicates the TG-binding site. The TG molecule, which is cocrystallized with the enzyme, is represented in a stick model.

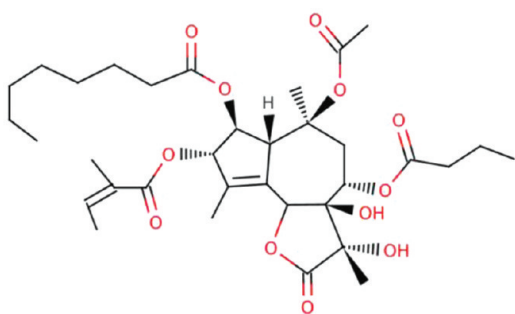


Figure 3. TG atomic structure. The molecule was drawn using Marvin 5.3.3, 2010, ChemAxon (<http://www.chemaxon.com>, accessed March 2, 2011).

include them. Positions of the missing insertions in the *PfATP6* models are indicated in Figure 5. It can be observed that the insertions occur in the cytoplasmatic domain (domain N, Figure 2) not affecting the TG-binding site, which is located in the transmembrane region.

Model Quality Assessment. The models of *PfATP6* and *SmSERCA* in both the E1 and E2 conformations, obtained as described in the Materials and Methods Section, are shown in Figure 5. Their quality was assessed using the new ProQM server,¹⁷ which is currently one of the best performing methods for quality assessment of transmembrane proteins while having an accuracy comparable to other methods for soluble proteins.¹⁷

The ProMQ results are visualized in Figure 5 where the per residue prediction accuracy score is color coded ranging from

blue (high predicted accuracy) to red (low predicted accuracy). The ProQM results for each model are also reported in Figure S1, Supporting Information, where the ProQM quality score (expressed as a numerical value in the range 0–1) is plotted along the protein sequence. Most of the residues and, in particular, the transmembrane helices that surround the TG binding cavity have a score ≥ 0.5 .

In order to better highlight domain conservation in the SERCA family, we performed a multiple sequence alignment across different levels of taxonomy. To this aim, we used the conserved domain architecture retrieval tool (CDART, <http://www.ncbi.nlm.nih.gov/Structure/lexington/lexington.cgi>, accessed May 16, 2011) to search for *PfSERCA* evolutionary conserved domains. Figure 4 shows the domain architecture of the SERCA family, and Figure 6 displays, for each domain, the corresponding multiple sequence alignment obtained from the most diverse 10 members of the family. From the figures it can be observed that the domain architecture as well as the single domain composition is well conserved across distantly related members of the SERCA family.

In conclusion, the SERCA transmembrane regions, which also include the regions responsible for binding TG in the mammalian protein, are very well conserved in both mammalian and parasite SERCAs (Figure 4) and, more generally, across different levels of taxonomy (Figures 4 and 6), do not contain insertions or deletions with respect to the template (Figure S2, Supporting Information), and therefore, their modeled conformation is expected to be very accurate, as indicated by the ProQM results.

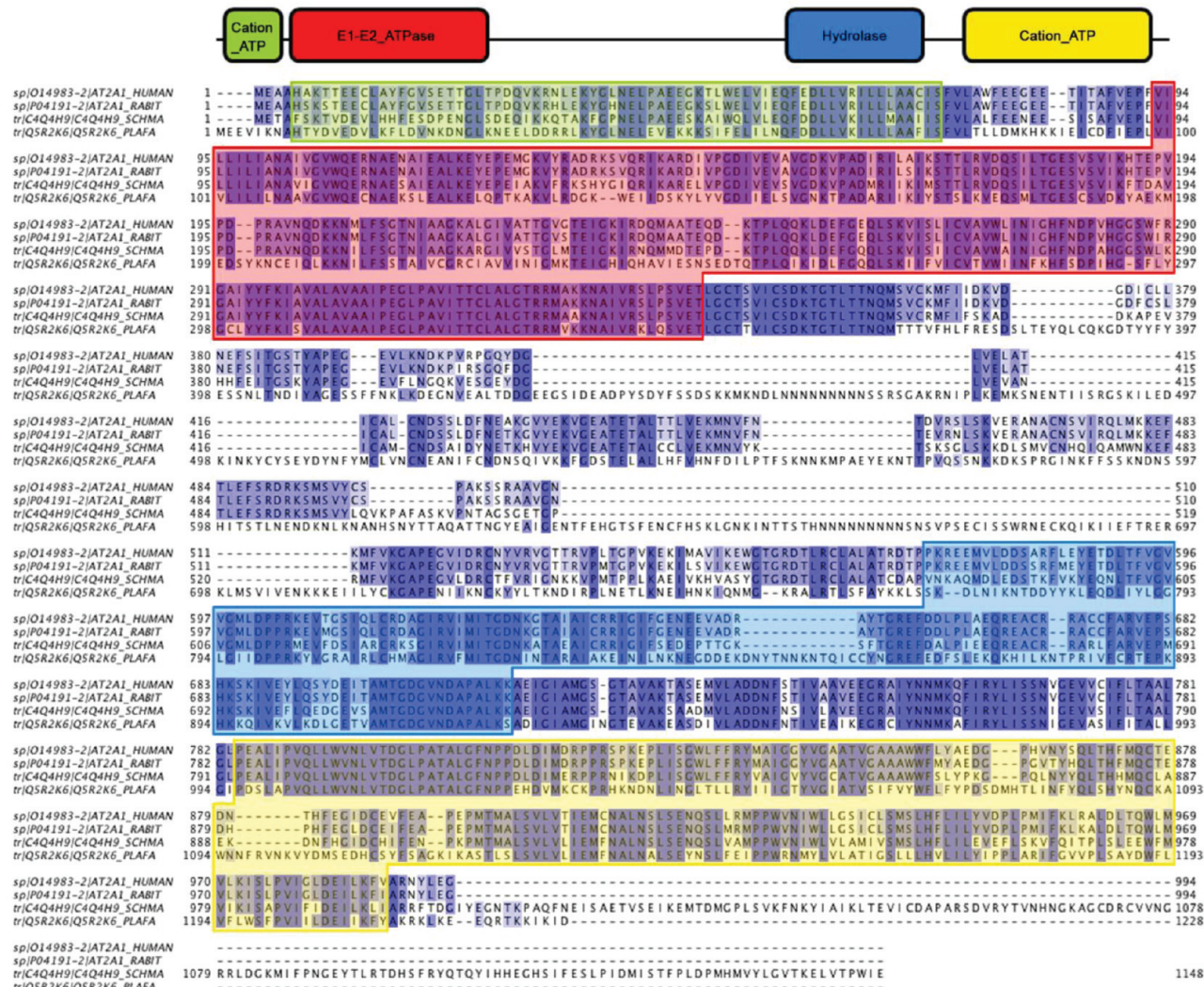


Figure 4. Domain architecture of the SERCA family and sequence alignment of *HsSERCA*, *OcSERCA*, *SmSERCA*, and *PfATP6*. Conserved regions are highlighted in blue. The domain architecture of the SERCA family obtained using CDART (<http://www.ncbi.nlm.nih.gov/Structure/lexington/lexington.cgi>) with the *PfATP6* sequence as input. Top: Domains are reported as colored rectangles. Bottom: Domains are highlighted in the multiple sequence alignment of *HsSERCA* (sp|O14983-2|AT2AI_HUMAN), *OcSERCA* (sp|P04191-2|AT2AI_RABIT), *SmSERCA* (tr|C4Q4H9|C4Q4H9_SCHMA), and *PfATP6* (tr|QSR2K6|QSR2K6_PLAFA) using the colors corresponding to the rectangles above. Pfam multiple sequence alignments of each SERCA family domain (Cation_ATPase N-terminus, E1-E2_ATPase, Hydrolase, and Cation_ATPase C-terminus) are reported in Figure 6.

Docking Studies. Docking of TG into the SmSERCA and PfATP6 Models. Docking simulations can be effectively used when the structure of the target protein is experimentally known or when it can be modeled with reasonable accuracy.^{29,30} At present, the goal of obtaining an accurate estimate of the quality of a protein model is still a rather elusive one in structural bioinformatics, and quality assessment tools are not yet completely reliable.³¹ Moreover, works that identified target-template sequence identity thresholds ensuring the usability of the corresponding comparative models in docking studies provide either general results^{32–35} or results for specific classes of proteins^{36–39} that might or might not apply to the case at hand. Therefore, we reasoned that the best way to assess whether our models are sufficiently accurate to be used as targets for docking experiments was to use them in a docking experiment with a known inhibitor for which information about the binding mode is available.

The structure of TG bound to the rabbit SERCA protein (Figure 2b) is available, and it is known that the molecule also

inhibits the homologous parasite proteins in the E2 state.^{26,40} It is expected that the binding sites in these proteins are similar, and therefore, we can verify whether our models are sufficiently accurate to permit docking of TG and identification of the correct binding site.

We docked TG to the models of *SmSERCA* and *PfATP6* in the E2 conformations using the protocol described in Materials and Methods Section. The results were very encouraging and reassured us that our models are of sufficient quality to be used for docking studies: The procedure, carried out blindly, i.e., without using any information other than the model structures, predicts as a binding site for TG the set of residues evolutionarily corresponding to those observed in the structure of the complex of rabbit SERCA and TG. Site-specific docking around the position identified in the blind docking was able to reconstruct a mode of interaction very similar to that observed in the experimental structure of the complex of the molecule with the mammalian protein. This can be appreciated in the

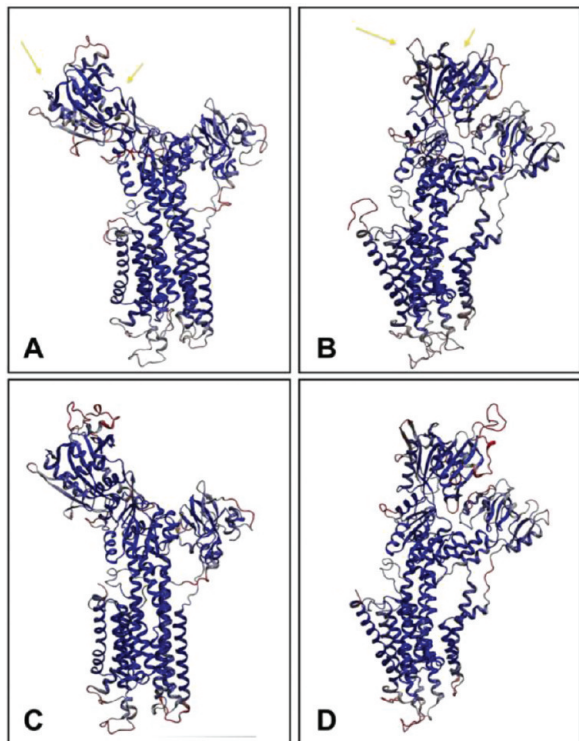


Figure 5. Structural models of the SERCA proteins. Residues of the models are colored according to the ProQM quality score ranging from blue (high predicted accuracy), to red (low predicted accuracy). The transmembrane region, which hosts the TG-binding site, is predicted to be highly accurate in all models. The arrows in light green indicate the positions of the two long insertions present in the *PfATP6* sequence (and not modeled). The longer arrow refers to the insertion between Leu382 and Arg473. The shorter one refers to the insertion between Asn569 and Cys677. (A) *PfATP6* in the calcium-bound state E1; (B) *PfATP6* in the calcium-free state E2; (C) *SmSERCA* in the calcium-bound state E1; and (D) *SmSERCA* in the calcium-free state E2.

two-dimensional diagrams [LIGPLOT (<http://www.ebi.ac.uk/thornton-srv/software/LIGPLOT/>, accessed March 2, 2011)] shown in Figure 7, reporting the TG-OcSERCA pattern of interactions observed in the experimentally determined co-crystal (Figure 7a) and the predicted interactions of TG with the structural model of both *PfATP6* and *SmSERCA* (Figure 7b and c, respectively). In particular, the LIGPLOT diagram shows that, in all three cases, TG establishes hydrophobic contacts with several residues of the M3, M5, and M7 helices (red arcs). A hydrogen bond is also present between the backbone of the isoleucine belonging to the L67 loop and the O8 atom of TG (dashed lines). Moreover, the computed energies are close to the observed values (*SmSERCA*: $\Delta E = -12.30$ kcal/mol, $K_i \sim 1$ nM; *PfATP6*: $\Delta E = -10.66$ kcal/mol, $K_i \sim 15$ nM).

Docking of Artemether into *PfATP6*. The artemisinin binding site on *PfATP6* has been experimentally determined,⁵ whereas no experimental data are specifically available for artemether. Binding modes and binding affinities of a number of artemisinin derivatives (including artemether) for *PfATP6* in the E2 state have been predicted by Naik and colleagues.⁴¹ In order to verify that our procedure is solid and capable of correctly predicting the artemether binding site with high accuracy and to verify if one conformational state is preferred over the other, we repeated the blind docking procedure using the artemether structure and the modeled structure

of *PfATP6* in both the E1 and E2 conformations. Our results indicate that the drug preferentially binds in the TG-binding cavity in both E1 and E2 states (Table 2). Nevertheless, the site-specific docking experiments show that the artemether pattern of interactions is different in the two states and that the drug has a stronger interaction with the *Plasmodium* target when the latter is in the E2 conformation (Figure 8). Incidentally, this is also the case for the binding of TG to the rabbit protein. TG binds OcSERCA in the E2 conformation because the absence of calcium causes an allosteric change, which induces the transmembrane binding pocket to become exposed to the drug. We believe that artemether prefers the *PfATP6* E2 conformation for the same reason.

In the E2 conformation, the residues of the M3, M5, and M7 helices form a surface that is nicely complementary to the artemether molecule (Figure 8b). In particular, the drug can establish several favorable hydrophobic interactions with the *PfATP6* transmembrane region by interacting with the Ile261, Leu263, Ile973, Ile977, Leu1040, and Ile1041 amino acid side chains. Other hydrophobic interactions are established with the backbone of Lys260 and Asn1039. Noticeably, the side chain of Phe264 is in an ideal position to allow a favorable stacking interaction of its phenyl group with the central cyclohexan and the six-membered eterocycle ring of the artemether tricyclic nucleus. In conclusion, the analysis of the binding energies provided by Autodock showed that the major energetic contributions came from hydrophobic and van der Waals interactions, whereas other electrostatic interactions, such as hydrogen bonds and salt bridges, were not observed.

Our results are consistent with data from mutational studies that identified the phenylalanine corresponding to Phe264 in mammalian SERCAs (Phe256) as a key residue for TG binding.⁴² In the calcium-bound state (E1), the latter interaction is not present (Figure 8a), and consistently, the calculated binding energy for the E2 conformation is lower than for E1 ($\Delta E = -8.66$ kcal/mol and $K_i = 0.5 \mu\text{M}$ for E2; $\Delta E = -7.43$ kcal/mol and $K_i = 3.6 \mu\text{M}$ for E1). Notice that the predicted K_i values compare very favorably with the experimental one observed for artemisinins, which is in the low micromolar range ($\sim 1-3 \mu\text{M}$).⁵

Docking of Artemether into *SmSERCA*. The next question we asked is whether a similarly convincing result would be obtained when docking artemether into *SmSERCA*, which would support our hypothesis that the latter protein is the molecular target of the drug.

This is indeed the case. Blind docking simulations of artemether into *SmSERCA* showed that, in both E1 and E2 conformational states, the best scoring ligand poses (see Materials and Methods Section) were localized in a region structurally equivalent to the one identified in *Plasmodium*, i.e., in the TG-binding cavity (Figure 7) and that the molecule establishes interactions similar to the ones observed in *PfATP6*. Also in this case, the binding region is composed by hydrophobic residues (Leu253, Phe256, Ile770, Ile774, Leu837, and Ile838), and in the calcium-free state of the protein, the orientation of artemether is very similar to that observed in the corresponding conformation of *PfATP6* (Figure 8d), and the interaction with the conserved Phe256 is preserved as well; neither hydrogen bonds nor salt bridges were observed. The predicted binding energy values ($\Delta E = -7.58$ and -7.61 kcal/mol for E1 and E2, respectively) and inhibition constants ($2.7 \mu\text{M}$ for both states) are similar for the two states and of the same order of magnitude of those computed for the *Plasmodium* protein. The higher energy value in the E2 state for binding of the drug into *SmSERCA* relative to *PfATP6*

a) Cation-ATPase N-terminus (PF00690)

91 122220787 59 HAYVEQELAURI. [12]. SRELAT TELESRYTYFERR. [1]. PPEQPTTFLYLRLDFRLLTTAGILS 135
91 6707665 143 NWLMPLETSAYSL. [8]. QNLUT FTEAKLROYGSNSL VSTKRSITVTLNEWLHPLFQANVSLW 214
91 82082056 152 EHDHTSAIHTKF GSBLTC SEGLSLRVICPENTI DVEVTPWLKLKEVNPYKFLFSCVLW 215
91 122011668 51 EKIGMETIELRL. [4]. ERBLKG DDFREFEFLYFSNOK. [1]. KSFESTKTYEFLLOCFDOMIRALVAVSLS 119
91 74764829 4 AFSKTYDEVLHVF. [4]. ENGLSD EQLRKIAKFEPPEN. [1]. AEEASRAIMOLVLFEDDLYKILLMAAIS 72
91 123416569 26 OTTGEVNEVATK. [4]. KRGESK NOLEGESKPYFNSV. [1]. VREVESTMFLDADDTKILCAACIS 94
91 15386272 37 QNFQBOQULLRN. [4]. FRKLIG. [2]. LARNSLRLKYSQNSM. [1]. INLAHARQYVSNSM. [1]. 134 RT. [1. 9]. LHETE. [2]. FOSL. [18]. S. [14]. SBS
91 268669296 152 VSHVTEPALAKSA. [1]. ASLKA DQVGLERLYFBNM. [1]. GFRKRSITVLLKEITQWFLINTLCSLF 72
91 148800923 4 FANTWDWVHL. [4]. YSLUKE PTVLHRRKXVRF. [1]. LRRSPRCYQAFRLKDPWVIVLVTISL 91
91 15116680 23 DKYQSTEGLEAKL. [4]. ATGLK 134 RT. [1. 9]. LHETE. [2]. FOSL. [18]. S. [14]. SBS
91 123628674 82 AVTTIVWGLVGDWDSRIGQ. [21]. NADELVNDVLLRAGDRVPADI.RLT. [3]. DPVVEWGTOMR 169
91 121730436 71 JMLLYSFALTEIEXQEVNLKLR. [21]. DASQYKEDPVLYVRGRKAPDVQVL. [1]. TGFDFRLITQES 156
91 81750231 338 3177LIGORLSERTATQSLLAE. [28]. PLQEYRNNDIVTAQSVTIVDQVVI. [2]. STRGASTIMHD 431
91 119270385 66 ILLATWTFSTLSSESSEFHQAHRD. [22]. RSESELVPQDWWNGEGEYVPRQYV. [2]. JAYDDEMOES 153
91 12778660 72 IFTYLLIFANTAEALARGAQAD. [22]. SSRRSLKDGYICEAGOTITPADEO. [2]. LASIDESQTE 159
91 119491134 603 FITLEFLARMEYSEKATGQAD. [36]. AYDLEQVNPISHEPASPADQV. [3]. IYQFDESQTEOS 705
91 126465500 87 LIFALYTSIELSEHARKLUS. [21]. RLDEWNVQDILVREKITYVPODQII. [2]. YSSFDTSVTOEA 173
91 319427642 169 ITAPMELGEYLEFESTASRDUMK. [21]. ATINNEWGQTYVAGAGLBYDQTMV. [2]. EANVFNASTQES 255
91 1519119107 476 7LILKQJNKTIVEVLTQYNSPAQ. [1]. 6L-QTRSLTKMVRQAGRCPCDQWV. [2]. STEVDTERIVSRQR. [1]. 548
91 153954843 184 LILALIDPNRVIKSUSKQKWL. [22]. SHHSVELDITVHSGELVPAQEVL. [2]. SSISETVSPQTQF 271
91 123628674 170 EM.RC. [1]. EGTTIPFAHTHVAEGAEVWVTTGMMTLDGODSPLL. [7]. QPLVNR. [2]. TAA. [2]. AA. 236
91 121730436 157 SEPTV. [1]. 6GRATIAESGATINQGTYVTRAYSPLESTV. [7]. GATORTLID. [2]. APYV. 223
91 81750231 432 QPTVK VDNTTQAGFNLVQDLSLQVTTTAAVSNR. [7]. NEPTNRL. [2]. AATL. [2]. VA. 497
91 119270385 154 EPEVK. [1]. KDRDVAQTRVGRORLREWEVAPGHSYDILMNL. [7]. MKESEVMS. [2]. LIGQEL. [2]. TF. 220
91 317478660 160 APTV. [4]. DKSSSTGTTKVISUKTKVUTQPGESFLDMIALV. [7]. TPNETALT. [2]. LAFT. [2]. VF. 229
91 119491134 706 KWKQV. [1]. AGHWTYVSKYINNEFLVYVTPKPSKSMDCD1INVV. [7]. APLEVRAD. [2]. TSHP. [2]. VI. 774
91 126465500 174 EPILL. [1]. RGRKQSYKVNKEFLVYVTPKPSKSMDCD1INVV. [7]. ASIOTKEF. [2]. AOPV. [2]. IV. 240
91 319427642 256 WATKR. [1]. RDTDVLSTGUVWEDQSR. RYAHVGTVTAALADYV. [7]. SPVOLQAS. [2]. ADKL. [2]. RV. 322
91 1519119107 549 NSAVK. [1]. MGDNVYATGTRVSYLSVYCOMINQTTIGISFL. [10]. PKLHRISN. [2]. LDIN. [2]. LY. 618
91 153954843 272 TVFP1. [1]. RGNHQJQTVWVLSNLKRITKIPQSVNODISSEQ 11LNKERV. [2]. QDRI. [2]. IA. 331

b) E1-E2_ATPase (PF00122)

91 123628674 24 FTDFEGW. [15]. AGYTRDVE 133
91 212639820 10 ICDFDGTI. [44]. IYVTSSTST DF. [5]. FRL. [2]. IYVTSSTST [4]. FLD. 113
91 162451092 30 ICDFDGTI. [44]. DRPAEALL DL. [5]. IBS. [2]. FHWISHGP LP FYIR. 129
91 269955980 5 VLDDFGTI. [29]. VSTLENSE EF. [5]. GYN. [2]. LATVSGSR SYV. 103
91 187520795 4 LVDFDGTI. [45]. RP. [1]. GOBL. [1]. KA. [1]. ENK. [2]. LEIVSGDV TYIK. 100
91 21195310 14 ICDFDGTI. [51]. FVTRSSK EV. [7]. NEVK. [7]. NVT. [2]. HYTSSGK ELIE. 126
91 281421888 10 LVDFDGTI. [52]. LSULTRSFQ KE. [7]. RGVK. [7]. EX. [4]. GLD. [2]. HYTSSGK EMIE. 123
91 8385753 9 IADYDFGTI. [52]. WFERFREDIE RH. [7]. PEVA. [8]. IV. [4]. GVR. [2]. HYTSSGK EMIA. 123
91 194336080 10 IADYDFGTI. [52]. WQVRSDFH KC. [7]. GVA. [7]. EX. [4]. NIR. [2]. HYTSSGK EMIE. 123
91 20723869 12 IWDDFGTI. [57]. GELDNLTR RL. [7]. PEVA. [7]. AW. [10]. DIK. [2]. HYTSSGK EMIE. 136

c) Hydrolase (PF00702)

91 123628674 134 RT. [1. 9]. LHETE. [2]. FOSL. [18]. S. [14]. SBS 134 RT. [1. 9]. LHETE. [2]. FOSL. [18]. S. [14]. SBS
91 212639820 114 GL. VEER. [2]. ONSA. [11]. P. [14]. KPS LLRLL. [1]. PRGATIVGUSLILDAKAI 191
91 162451092 130 GPETV. [2]. GPEV. [2]. VETV. [2]. VETV. [2]. VETV. [2]. VETV. [2]. VETV. 196
91 269955980 104 SV. [6]. IPVVS. [2]. DDVX. [5]. I. [14]. REA VND. [1]. KZDDEAWFLGNTSDRRAE. 171
91 187520795 101 PF. [5]. LSOFF. [2]. CANG. [6]. I. [10]. KLA. [5]. RVRV. [1]. ALGVKTYVGDNSDVKAAI 169
91 18155310 127 GT. [3]. PEFFER. [2]. PEFFER. [2]. PEFFER. [2]. PEFFER. [2]. PEFFER. [2]. PEFFER. 211
91 281421888 124 GT. [3]. HEFEN. [2]. ACSE. [10]. P. [14]. KIN. [5]. VSDON. [12]. IPFPRVIVYFQGGETDPCMR 209
91 8385753 124 AS. [3]. KEDFA. [2]. ASEF. [10]. A. [14]. RIN. [5]. LSDHA. [12]. VPF RMYVQGQDGTDPCMR 209
91 194336080 124 GT. [3]. KETFA. [2]. ASOF. [10]. P. [14]. RIN. [5]. VDONS. [12]. VPF RMYVQGQDGTDPCMR 209
91 20723869 137 GS. [3]. PHDQ. [2]. QCEF. [14]. V. [14]. EIN. [5]. HPEAV. [12]. VPF AMVYVADPSDPAFS 226V

d) Cation-ATPase C-terminus (PF00689)

91 123628674 874 PLTFLICLQDGTDCTPCTTETDINTKRP. [2]. KSHPLVQKRFVFTA. [1]. LONGFLSTY. [2]. F. 940
91 12470165 774 YNQTOQLIWTFIDTFAFMTEIPLSRLYEQ. [1]. ERYHLTHNMWANI ISQIVYQLL. [2]. F. 938
91 122155040 603 PLSATELFLVNLVDSLALATESEMEWNPQ. [1]. NAEELLTSTMRVAI FQIVVQLL. [2]. J. 575
91 75209999 510 [2]. VITAVQQLWANLINDSGLALATDPAKNDVLP. [2]. RSEASLJAFQELRN. LIVAFVQQL. [2]. J. 575
91 14825742 999 [2]. VITAVQQLWANLINDSGLALATDPAKNDVLP. [2]. RSEASLJAFQELRN. LQGQATQVY. [2]. F. 1084
91 123472220 746 [2]. PLPKTQIQLWNLINDSGLALATRPSLSSLKH. [2]. EGINLISNLTARNM SIQIVYQLL. [2]. J. 811
91 152828953 839 [2]. PLKAVQQLWANLINDTASLATMPTDILLKRP. [2]. KTPPLISTMKNNI LQQAVQQLV. [2]. F. 904
91 126465500 745 [2]. PMRAQQLWNLINDSGLALATRPSLSSLDRPP. [2]. SASKLISLURNI AHQHFOQA. [2]. M. 810
91 22504333 730 [2]. PFKAVQQLWNLINDSGLALATRPSLSSLDRPP. [2]. KODPLUDSFLURNI 19QSVLQIL. L. 793
91 1519119107 691 [2]. PLNVAQQLWNLINDSGLALATRPSLSSLDRPP. [2]. KDFLQVYVLMR. L. 793
91 151912221 691 [2]. PLNVAQQLWNLINDSGLALATRPSLSSLDRPP. [2]. KDFLQVYVLMR. L. 793
91 124453510 874 TFLYQIUVQQLWANL. YGLR. S. [4]. GSFLQ. [2]. S. [26]. VEGTR. 1125
91 12470165 839 MQLQSTQ. [17]. H. TLLNTFQYQQLQIEN. [1]. LISHK QNCR. K. [8]. NNKR. [2]. T. [31]. IFNLS. 936
91 122155040 668 YILDEDFGP. [1]. D. TOIQGCFWMLQAN ELESSR. R. [9]. SGHL
91 75209999 576 LMIFQVNG. [31]. Y. TCIXNFFIAQFLN LIPTR. [15]. Q. 1064
91 14825742 1065 VLFHAGQD. [15]. Q. AMTENTVWLOQWK. L. 116
91 123472220 812 LILFRQK. [17]. V. SWMFTNFWMTFVNEN LINSR. V. [8]. DQIQL H. [24]. VFTV. 899
91 152828953 905 GLLFGW. [19]. F. TLLNFWMTFVNEN LINAR. K. [4]. RMIF. Q. [5]. AFSTK. 971
91 1243430732 874 [2]. PMRAQQLWNLINDSGLALATRPSLSSLDRPP. [2]. KDFLQVYVLMR. V. [8]. EGFL S. [24]. VFTV. 893
91 12504333 730 [2]. PFKAVQQLWNLINDSGLALATRPSLSSLDRPP. [2]. KDFLQVYVLMR. L. 793
91 1519119107 794 IGYVLFPE. [10]. Y. TFFENSFWMQQIFN LINAR. [1]. S. [7]. DQIQL D. [24]. VFTV. 874
91 151912221 757 VLFEPF. [9]. S. GEMTFCOQFN FINNY. S. [7]. FRIIF K. [24]. FFKL. 855

Figure 6. Multiple alignments of the SERCA family domains. (a) Multiple sequence alignment of Cation-ATPase N-terminus (PF00690) domain including the 10 most diverse members of the family; (b) multiple sequence alignment of E1-E2_ATPase (PF00122) domain including the 10 most diverse members of the family; (c) multiple sequence alignment of Hydrolase (PF00702) domain including the 10 most diverse members of the family; and (d) multiple sequence alignment of Cation-ATPase C-terminus (PF00689) domain including the 10 most diverse members of the family.

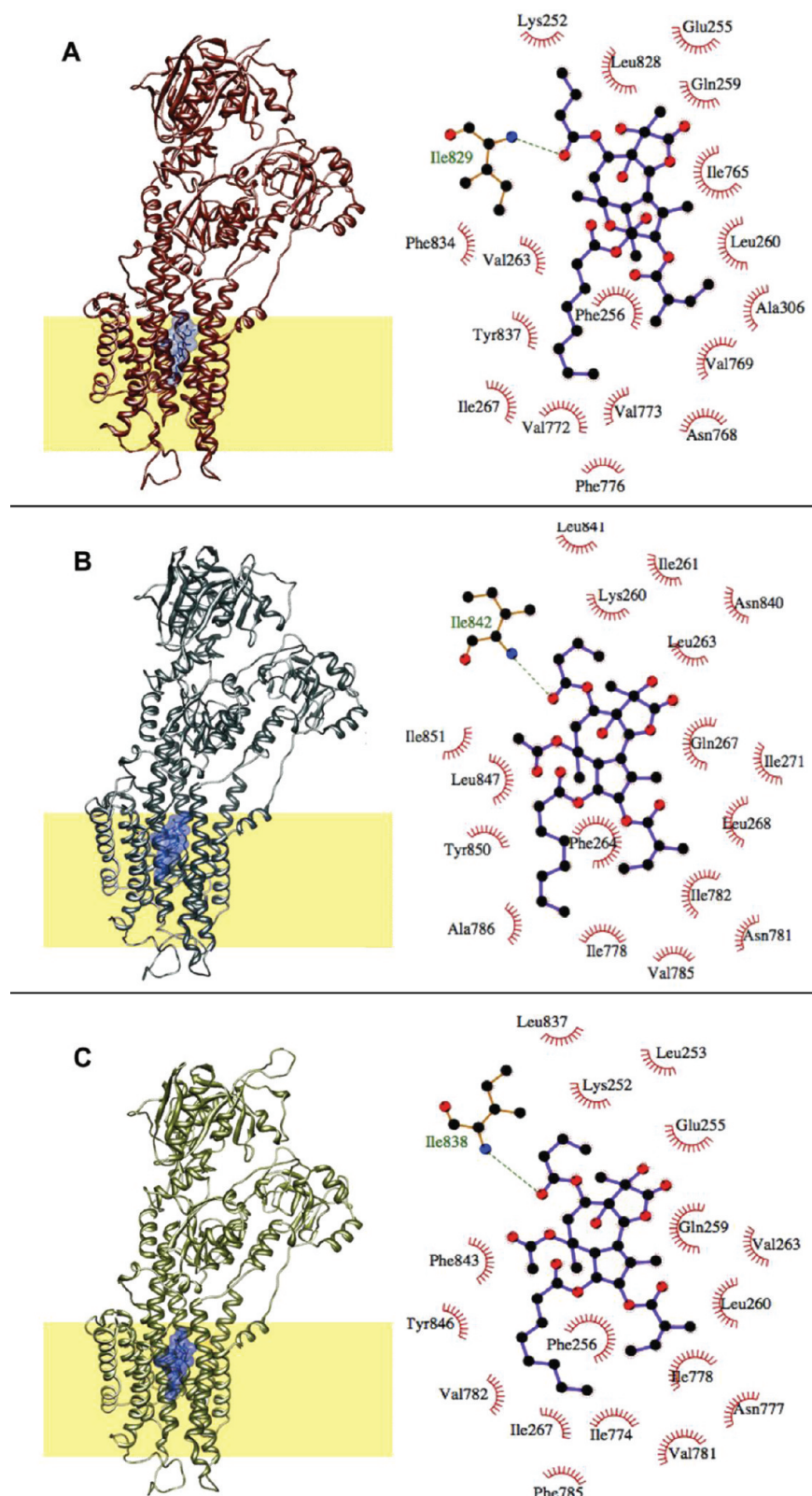


Figure 7. Observed and predicted TG-binding site. (A) The TG-binding site as observed in the OcSERCA-TG cocrystal (left) and the corresponding LIGPLOT diagram (right); (B) the TG-binding site in *PfATP6* and (C) *SmSERCA* models predicted by the blind docking experiment (left) and the corresponding LIGPLOT diagram resulting from the site-specific docking (see Materials and Methods Section). LIGPLOT is a program that plots schematic diagrams of protein–ligand interactions. The interactions shown are those mediated by hydrogen bonds and by hydrophobic contacts. Hydrogen bonds are indicated by dashed lines between the atoms involved, while hydrophobic contacts are represented by an arc with spokes radiating toward the ligand atoms they contact (<http://www.ebi.ac.uk/thornton-srv/software/LIGPLOT/>, accessed March 2, 2011).

Table 2. Results of the Blind Docking Experiments of Artemether into the Modelled Structure of *PfATP6*, *SmSERCA*, and *HsSERCA* in Both the E1 and E2 Conformations

enzyme	number of conformations (out of 200) in the cluster located in the TG binding site ^a	energy kcal/mol	average number of conformations ^b	standard deviation ^c
<i>PfATP6</i> E1	49	-7.43	15.1 (151/10)	23.7
<i>PfATP6</i> E2	182	-8.66	2.2 (18/8)	1.6
<i>SmSERCA</i> E1	58	-7.58	15.7 (142/9)	38.4
<i>SmSERCA</i> E2	75	-7.61	15.6 (125/8)	24.5
<i>HsSERCA</i> E1	50	-7.83	21.4 (150/7)	35.4
<i>HsSERCA</i> E2	172	-8.37	5.6 (28/5)	7.0

^a Number of poses located in the cavity surrounded by the M3, M5, and M7 transmembrane helices, corresponding to the TG binding region. The total number of runs was 200. ^b Average number of conformations per clusters excluding those located in the TG binding region. ^c Standard deviation was calculated taking into account all conformations but the ones located in the TG binding region.

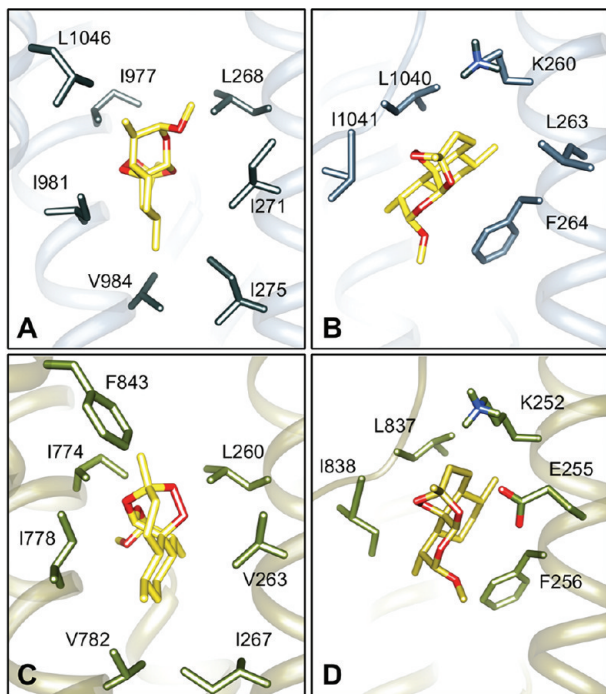


Figure 8. Predicted artemether binding sites in *PfATP6* and *SmSERCA*. The artemether molecule is represented in sticks. The transmembrane helices belonging to the binding cavity are represented as ribbons. Residues involved in the interaction with artemether are represented in sticks. The artemether binding site in the model of *PfATP6* (A) in state E1 and (B) in state E2. The artemether binding site in the model of *SmSERCA* (C) in state E1 and (D) in state E2.

can be rationalized by the presence of Glu255 near the *SmSERCA* binding pocket, in a spatial position that is occupied by Leu263 in *PfATP6*.

As a control experiment, we also carried out docking simulations using as a target an enzyme of known structure (PDB: 2X8C) in the detoxification pathway of *S. mansoni*, the thioredoxin glutathione reductase (*SmTGR*), which is inhibited by auranofin⁴³ and 1,2,5-oxadiazole 2-oxide (furoxan)⁴⁴ but not by artemether. Blind docking experiments of artemether into the structure of this enzyme with the same procedure and parameters used here for SERCAs provided no solutions near the active site, the NADPH binding site, and/or the C-terminal tail of the enzyme, a region involved in

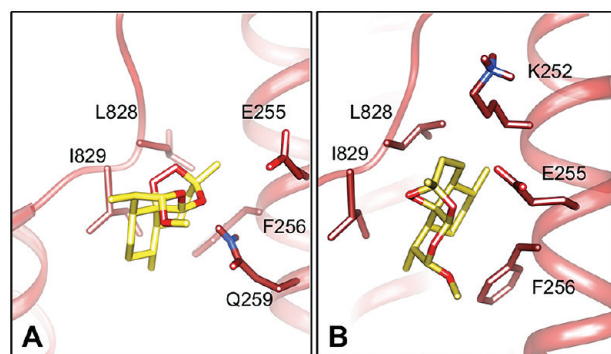


Figure 9. Predicted artemether binding site in *HsSERCA*. The artemether binding site in the model of *HsSERCA* (A) in state E1 and (B) in the E2. The artemether molecule is represented in sticks. The transmembrane helices belonging to the binding cavity are represented as ribbons. *HsSERCA* residues involved in the interaction with artemether are in sticks.

catalysis⁴⁵ (data not shown). Incidentally, this was not the case when auranofin and furoxan were docked into *SmTGR* (manuscript in preparation).

Analysis of the Different Pharmacological Activity of Artemether in the Parasites and in Humans. As mentioned in the Introduction Section, artemisinin and its derivatives, including artemether, cause no adverse reactions or noticeable side effects in humans. On the other hand, extracts from plants rich in sesquiterpene lactones have gained considerable interest for treating human diseases, such as inflammations and infections. The sesquiterpene lactone-derived drugs from TG and artemisinin are now being tested in cancer clinical trials, and their effectiveness as anticancer molecule is attributed to their ability to target the sarco/endoplasmic reticulum calcium ATPase pump.^{11,46}

To reconcile these observations and assess whether they can be related to the difference in the structure of the human protein (*HsSERCA*), we built a model for this protein and repeated the docking analysis also in this case.

Docking of Artemether into *HsSERCA*. Interestingly, there is no structural difference in the predicted binding site between the human protein and the parasite ones. Also in this case, artemether binds preferentially to the TG-binding cavity (Table 2) even though it establishes a different pattern of hydrophobic interactions with the residues of the protein in states E1 and E2 (Figure 9a and b). In state E1, the position of artemether in the

Table 3. Residues of *PfATP6*, *SmSERCA*, and *HsSERCA* That Establish Favorable Interactions with the Artemether Molecule in State E2

	M3	M5	M7
<i>PfATP6</i>	K260 I261 L263 F264 I973 I977 N1039 L1040 I1041		
<i>SmSERCA</i>	K252 L253 E255 F256 I770 I774 P836 L837 I838		
<i>HsSERCA</i>	K252 L253 E255 F256 I761 I765 P827 L828 I829		

TG-binding cavity is shifted toward the extracellular part of the cavity with respect to the corresponding conformation in *PfATP6* and *SmSERCA*. Similarly to the *PfATP6* case, binding is stronger in the E2 conformation, and several hydrophobic interactions are established between residues belonging to the M3 (Lys252, Leu253, Glu255, Phe256), M5 (Ile761, Ile765), and M7 (Leu828, Ile829) helices of *HsSERCA* and the artemether molecule (Figure 9). Similarly to the cases of *PfATP6* and *SmSERCA*, only hydrophobic and van der Waals interactions were observed. The interaction between *HsSERCA* Phe256 and the sesquiterpene ring of the artemether is preserved as well, both in terms of atom distances and orientations. Consistently, the computed parameters for the binding of the drug are only moderately lower than those found for the parasite proteins ($\Delta E = -8.37 \text{ kcal/mol}$ and $K_i = 0.7 \mu\text{M}$ for E2, and $\Delta E = -7.83 \text{ kcal/mol}$ and $K_i = 1.8 \mu\text{M}$ for E1).

Our docking simulations indicate that there is no obvious reason for the lack of inhibition of the drug for the human protein and strongly support the hypothesis that the molecule can bind to both parasite and mammalian SERCA proteins. We believe that its different pattern of activity is related to the cellular context, as discussed later.

Specific Cellular Context Accounts for the Different Pharmacological Activity of Artemether Observed in the Parasites and in Humans. As mentioned before, it has been proposed that the single Leu263Glu mutation in *PfATP6* is responsible for the different sensitivity of *P. falciparum* and mammals to artemisinins.²⁴ This observation is however in contrast with the finding that parasite clones containing the Leu263Glu mutation do not show a significant decreased sensitivity to artemisinins.²⁵ Furthermore, it is known that artemisinins kill *S. mansoni*,⁴⁷ and we show here that this is very likely due to binding of the molecule to *SmSERCA*, which does have a glutamic acid in the position corresponding to *PfATP6* Leu263 (Table 3). Moreover artemisinins do inhibit *HsSERCA* in human cancer cells in an iron-dependent fashion.^{9,11,48}

These observations can be reconciled by noticing that artemisinins contain an endoperoxide bridge, which is known to be responsible for the drug activation by Fe^{2+} ions.⁶ The bridge is absent in the TG molecule, and indeed this molecule, although expected to bind in a similar fashion to the SERCA enzymes of *P. falciparum*, *S. mansoni*, and *H. sapiens*, exerts its action independently on the presence of iron⁵ and, in humans, is not selective for cancer versus normal cells.⁴⁶

Our analysis supports the conclusion that the differential sensitivity of SERCAs to artemether is not related to differences in the artemether binding mode in the parasite and mammalian targets, as suggested by Uhlemann and collaborators,²⁴ but rather to the specific cellular context and, in particular, to the iron concentration that activates the molecule in infected erythrocytes and in cancer cells, consistently with what has been proposed by several authors. $\text{Fe}(\text{II})$ might activate the molecule in the developmental stages of the parasites that occur in abundant

iron source (provided, for example, by the infected erythrocytes in the case of *Plasmodium*) and in most cancer cells which, compared to normal cells, have high rates of iron intake^{10,49} and express a high surface concentration of transferrin receptors.⁵⁰

CONCLUSIONS

Computational tools, such as comparative modeling and docking simulations, have reached a sufficient degree of maturity to be useful not only to rationalize experimental observations but also to propose new mechanisms and foster scientific discoveries.

One of the strengths of computational biology is the ability to address a range of problems using similar computational tools. Because of this, it cannot be expected that every prediction is experimentally verified by the scientists proposing it, and indeed, the experimental verification of our hypothesis goes beyond the scope of our work. However, we believe that it is important, in cases such as this, to suggest specific experiments to the experimental community interested in the problem at hand.

Here we put forward and provide support for a hypothesis that can be readily tested by scientists working on *Schistosoma*; the molecular target of artemether in *Schistosoma* is the SERCA protein of the parasite and the binding site of the drug overlaps with that of TG.

We also provide a putative explanation for the different pharmacological activity of artemether against the parasite and human proteins which could be tested by analyzing the sensitivity of *HsSERCA* to artemether as a function of iron concentration.

ASSOCIATED CONTENT

S Supporting Information. Figure S1 reports results of ProQM for the *PfATP6* and *SmSERCA* models in the E1 and E2 conformational states, and Figure S2 is the target-template sequence alignments for *PfATP6*, *SmSERCA*, and *HsSERCA*. This material is available free of charge via the Internet at <http://pubs.acs.org>.

AUTHOR INFORMATION

Corresponding Author

*E-mail: anna.tramontano@uniroma1.it; allegra.via@uniroma1.it.

ACKNOWLEDGMENT

We thank all our colleagues of the Biocomputing Unit and the members of the Fondazione Roma Research Unit led by Prof. Maurizio Brunori for useful discussions. This work was partially supported by award number KUK-I1-012-43 made by King Abdullah University of Science and Technology (KAUST), Human Frontier Science Program HFSP-RGP0054/2006-C grant (<http://www.hfsp.org/>), FIRB Italbionet and Proteomica, Ministry of Health grant contract no. Onc_Ord 25/07, Fondazione Roma, and the IIT SEED project “Advanced Computational Methods for Biophysics, Drug Design, and Energy Research”.

REFERENCES

- (1) al-Waili, N. S. Praziquantel for treatment of malaria. *JPMA, J. Pak. Med. Assoc.* **1998**, *48* (12), 378–379.
- (2) Utzinger, J.; Xiao, S.; N’Goran, E. K.; Bergquist, R.; Tanner, M. The potential of artemether for the control of schistosomiasis. *Int. J. Parasitol.* **2001**, *31* (14), 1549–1562.

- (3) Olliaro, P. L.; Haynes, R. K.; Meunier, B.; Yuthavong, Y. Possible modes of action of the artemisinin-type compounds. *Trends Parasitol.* **2001**, *17* (3), 122–126.
- (4) White, N. J. Qinghaosu (artemisinin): the price of success. *Science* **2008**, *320* (5874), 330–334.
- (5) Eckstein-Ludwig, U.; Webb, R. J.; Van Goethem, I. D.; East, J. M.; Lee, A. G.; Kimura, M.; O'Neill, P. M.; Bray, P. G.; Ward, S. A.; Krishna, S. Artemisinins target the SERCA of Plasmodium falciparum. *Nature* **2003**, *424* (6951), 957–961.
- (6) Krishna, S.; Uhlemann, A. C.; Haynes, R. K. Artemisinins: mechanisms of action and potential for resistance. *Drug Resist. Updates* **2004**, *7* (4–5), 233–244.
- (7) Taylor, W. R.; White, N. J. Antimalarial drug toxicity: a review. *Drug Saf.* **2004**, *27* (1), 25–61.
- (8) Singh, N. P.; Panwar, V. K. Case report of a pituitary macroadenoma treated with artemether. *Integr. Cancer Ther.* **2006**, *5* (4), 391–394.
- (9) Singh, N. P.; Lai, H. Selective toxicity of dihydroartemisinin and holotransferrin toward human breast cancer cells. *Life Sci.* **2001**, *70* (1), 49–56.
- (10) Shterman, N.; Kupfer, B.; Moroz, C. Comparison of transferrin receptors, iron content and isoferitin profile in normal and malignant human breast cell lines. *Pathobiology* **1991**, *59* (1), 19–25.
- (11) Stockwin, L. H.; Han, B.; Yu, S. X.; Hollingshead, M. G.; ElSohly, M. A.; Gul, W.; Slade, D.; Galal, A. M.; Newton, D. L.; Bumke, M. A. Artemisinin dimer anticancer activity correlates with heme-catalyzed reactive oxygen species generation and endoplasmic reticulum stress induction. *Int. J. Cancer* **2009**, *125* (6), 1266–1275.
- (12) Soding, J.; Biegert, A.; Lupas, A. N. The HHpred interactive server for protein homology detection and structure prediction. *Nucleic Acids Res.* **2005**, *33*, (Web Server issue), W244–248.
- (13) Soding, J. Protein homology detection by HMM-HMM comparison. *Bioinformatics* **2005**, *21* (7), 951–960.
- (14) Rose, P. W.; Beran, B.; Bi, C.; Bluhm, W. F.; Dimitropoulos, D.; Goodsell, D. S.; Prlic, A.; Quesada, M.; Quinn, G. B.; Westbrook, J. D.; Young, J.; Yukich, B.; Zardecki, C.; Berman, H. M.; Bourne, P. E. The RCSB Protein Data Bank: redesigned web site and web services. *Nucleic Acids Res.* **39**, (Database issue), D392–401.
- (15) Sali, A.; Blundell, T. L. Comparative protein modelling by satisfaction of spatial restraints. *J. Mol. Biol.* **1993**, *234* (3), 779–815.
- (16) Shen, M. Y.; Sali, A. Statistical potential for assessment and prediction of protein structures. *Protein Sci.* **2006**, *15* (11), 2507–2524.
- (17) Ray, A.; Lindahl, E.; Wallner, B. Model quality assessment for membrane proteins. *Bioinformatics* **26**, (24), 3067–3074.
- (18) Castrignano, T.; De Meo, P. D.; Cozzetto, D.; Talamo, I. G.; Tramontano, A., The PMDB Protein Model Database. *Nucleic Acids Res.* **2006**, *34*, (Database issue), D306–309.
- (19) Toyoshima, C.; Nomura, H. Structural changes in the calcium pump accompanying the dissociation of calcium. *Nature* **2002**, *418* (6898), 605–611.
- (20) Toyoshima, C.; Nakasako, M.; Nomura, H.; Ogawa, H. Crystal structure of the calcium pump of sarcoplasmic reticulum at 2.6 Å resolution. *Nature* **2000**, *405* (6787), 647–655.
- (21) Allen, F. H. The Cambridge Structural Database: a quarter of a million crystal structures and rising. *Acta Crystallogr., Sect. B* **2002**, *58* (Pt 3 Pt 1), 380–388.
- (22) Morris, G. M.; Huey, R.; Lindstrom, W.; Sanner, M. F.; Belew, R. K.; Goodsell, D. S.; Olson, A. J. AutoDock4 and AutoDockTools4: Automated docking with selective receptor flexibility. *J. Comput. Chem.* **2009**, *30* (16), 2785–2791.
- (23) Pettersen, E. F.; Goddard, T. D.; Huang, C. C.; Couch, G. S.; Greenblatt, D. M.; Meng, E. C.; Ferrin, T. E. UCSF Chimera—a visualization system for exploratory research and analysis. *J. Comput. Chem.* **2004**, *25* (13), 1605–1612.
- (24) Uhlemann, A. C.; Cameron, A.; Eckstein-Ludwig, U.; Fischbarg, J.; Iserovich, P.; Zuniga, F. A.; East, M.; Lee, A.; Brady, L.; Haynes, R. K.; Krishna, S. A single amino acid residue can determine the sensitivity of SERCAs to artemisinins. *Nat. Struct. Mol. Biol.* **2005**, *12* (7), 628–629.
- (25) Valderramos, S. G.; Scanfeld, D.; Uhlemann, A. C.; Fidock, D. A.; Krishna, S., Investigations into the role of the Plasmodium falciparum SERCA (PfATP6) L263E mutation in artemisinin action and resistance. *Antimicrob. Agents Chemother.* **54**, (9), 3842–3852.
- (26) Cunha, V. M.; Reis, J. M.; Noel, F. Evidence for the presence of two (Ca²⁺-Mg²⁺) ATPases with different sensitivities to thapsigargin and cyclopiazonic acid in the human flatworm Schistosoma mansoni. *Comp. Biochem. Physiol., Part B: Biochem. Mol. Biol.* **1996**, *114* (2), 199–205.
- (27) Ward, J. J.; Sodhi, J. S.; McGuffin, L. J.; Buxton, B. F.; Jones, D. T. Prediction and functional analysis of native disorder in proteins from the three kingdoms of life. *J. Mol. Biol.* **2004**, *337* (3), 635–645.
- (28) Dosztanyi, Z.; Csizmok, V.; Tompa, P.; Simon, I. The pairwise energy content estimated from amino acid composition discriminates between folded and intrinsically unstructured proteins. *J. Mol. Biol.* **2005**, *347* (4), 827–839.
- (29) Kairys, V.; Gilson, M. K.; Fernandes, M. X. Using protein homology models for structure-based studies: approaches to model refinement. *TheScientificWorldJournal* **2006**, *6*, 1542–1554.
- (30) Cavasotto, C. N.; Phatak, S. S. Homology modeling in drug discovery: current trends and applications. *Drug Discovery Today* **2009**, *14* (13–14), 676–683.
- (31) Cozzetto, D.; Kryshtafovych, A.; Tramontano, A. Evaluation of CASP8 model quality predictions. *Proteins* **2009**, *77* (Suppl 9), 157–166.
- (32) Baker, D.; Sali, A. Protein structure prediction and structural genomics. *Science* **2001**, *294* (5540), 93–96.
- (33) Fan, H.; Irwin, J. J.; Webb, B. M.; Klebe, G.; Shoichet, B. K.; Sali, A. Molecular docking screens using comparative models of proteins. *J. Chem. Inf. Model.* **2009**, *49* (11), 2512–2527.
- (34) Oshiro, C.; Bradley, E. K.; Eksterowicz, J.; Evensen, E.; Lamb, M. L.; Lanctot, J. K.; Putta, S.; Stanton, R.; Grootenhuis, P. D. Performance of 3D-database molecular docking studies into homology models. *J. Med. Chem.* **2004**, *47* (3), 764–767.
- (35) Kairys, V.; Fernandes, M. X.; Gilson, M. K. Screening drug-like compounds by docking to homology models: a systematic study. *J. Chem. Inf. Model.* **2006**, *46* (1), 365–379.
- (36) Bissantz, C.; Bernard, P.; Hibert, M.; Rognan, D. Protein-based virtual screening of chemical databases. II. Are homology models of G-Protein Coupled Receptors suitable targets? *Proteins* **2003**, *50* (1), 5–25.
- (37) Lowrie, J. F.; Delisle, R. K.; Hobbs, D. W.; Diller, D. J. The different strategies for designing GPCR and kinase targeted libraries. *Comb. Chem. High Throughput Screen.* **2004**, *7* (5), 495–510.
- (38) Fernandes, M. X.; Kairys, V.; Gilson, M. K. Comparing ligand interactions with multiple receptors via serial docking. *J. Chem. Inf. Comput. Sci.* **2004**, *44* (6), 1961–1970.
- (39) McGovern, S. L.; Shoichet, B. K. Information decay in molecular docking screens against holo, apo, and modeled conformations of enzymes. *J. Med. Chem.* **2003**, *46* (14), 2895–2907.
- (40) Varotti, F. P.; Beraldo, F. H.; Gazarini, M. L.; Garcia, C. R. Plasmodium falciparum malaria parasites display a THG-sensitive Ca²⁺ pool. *Cell Calcium* **2003**, *33* (2), 137–144.
- (41) Naik, P. K.; Srivastava, M.; Bajaj, P.; Jain, S.; Dubey, A.; Ranjan, P.; Kumar, R.; Singh, H., The binding modes and binding affinities of artemisinin derivatives with Plasmodium falciparum Ca²⁺-ATPase (PfATP6). *J. Mol. Model.* **17**, (2), 333–357.
- (42) Xu, C.; Ma, H.; Inesi, G.; Al-Shawi, M. K.; Toyoshima, C. Specific structural requirements for the inhibitory effect of thapsigargin on the Ca²⁺ ATPase SERCA. *J. Biol. Chem.* **2004**, *279* (17), 17973–17979.
- (43) Simeonov, A.; Jadhav, A.; Sayed, A. A.; Wang, Y.; Nelson, M. E.; Thomas, C. J.; Inglese, J.; Williams, D. L.; Austin, C. P. Quantitative high-throughput screen identifies inhibitors of the Schistosoma mansoni redox cascade. *PLoS Neglected Trop. Dis.* **2008**, *2* (1), e127.
- (44) Sayed, A. A.; Simeonov, A.; Thomas, C. J.; Inglese, J.; Austin, C. P.; Williams, D. L. Identification of oxadiazoles as new drug leads for the control of schistosomiasis. *Nat. Med.* **2008**, *14* (4), 407–412.

- (45) Angelucci, F.; Sayed, A. A.; Williams, D. L.; Boumis, G.; Brunori, M.; Dimastrogiovanni, D.; Miele, A. E.; Pauly, F.; Bellelli, A. Inhibition of *Schistosoma mansoni* thioredoxin-glutathione reductase by auranofin: structural and kinetic aspects. *J. Biol. Chem.* **2009**, *284* (42), 28977–28985.
- (46) Denmeade, S. R.; Isaacs, J. T. The SERCA pump as a therapeutic target: making a “smart bomb” for prostate cancer. *Cancer Biol. Ther.* **2005**, *4* (1), 14–22.
- (47) Xiao, S.; Tanner, M.; N’Goran, E. K.; Utzinger, J.; Chollet, J.; Bergquist, R.; Chen, M.; Zheng, J. Recent investigations of artemether, a novel agent for the prevention of schistosomiasis japonica, mansoni and haematobia. *Acta Trop.* **2002**, *82* (2), 175–181.
- (48) Lu, J. J.; Chen, S. M.; Zhang, X. W.; Ding, J.; Meng, L. H. The anti-cancer activity of dihydroartemisinin is associated with induction of iron-dependent endoplasmic reticulum stress in colorectal carcinoma HCT116 cells. *Invest. New Drugs* **2010**, *29* (6), 1276–1283.
- (49) Karin, M.; Mintz, B. Receptor-mediated endocytosis of transferrin in developmentally totipotent mouse teratocarcinoma stem cells. *J. Biol. Chem.* **1981**, *256* (7), 3245–3252.
- (50) May, W. S., Jr.; Cuatrecasas, P. Transferrin receptor: its biological significance. *J. Membr. Biol.* **1985**, *88* (3), 205–215.